Journal of Applied Fluid Mechanics, Vol. 12, No. 5, pp. 1417-1428, 2019.
Available online at www.jafmonline.net, ISSN 1735-3645, EISSN 1735-3645.
DOI: 10.29252/jafm.12.05.29329

Experimental Study of the Effect of Displacement of Vanes Submerged at Channel Width on Distribution of Velocity and Shear Stress in a 180 Degree Bend

Ch. Abdi Chooplou and M. Vaghefi †

Civil Engineering Department, Persian Gulf University, Bushehr, 7516913817, Iran

†*Corresponding Author Email: vaghefi@pgu.ac.ir*

(Received June 30, 2018; accepted January 12, 2019)

ABSTRACT

Shear stress is a parameter of high significance. Through knowledge of this parameter, assessment of scour or sedimentations at different points of bed is made viable. Therefore, this paper investigated alterations in shear stress along the bend, specifically around a bridge pier, under the influence of applying submerged vanes at the upstream side of the bridge pier. With the aim of modeling submerged vanes, vanes of Plexiglas with a thickness of 20% of the pier diameter, a length of 1.5 times the pier diameter, and submergence ratio of 75% were utilized. The vanes were installed at a distance equal to 5 times the pier diameter from the pier center at a distance of 40 to 60% of the channel width from the inner bank at the upstream side of the bridge pier. Acoustic-Doppler Velocity velocimeter device was utilized for measuring three-dimensional velocity components. The experiments were conducted in a 1-meter-wide flume with a degree of curvature of 180. The results of the study suggested that upon reaching the bend apex, the maximum flow turbulence rate occurred in a transverse direction in the case of installing submerged vanes at a distance of 40% of the channel width from the inner bank towards the inner wall; while in the case of installing submerged vanes at a distance of 60% of the channel width from the inner bank, it occurred towards the outer wall, and it could be observed that the maximum longitudinal and vertical components of turbulence rate increased by 16 and 5.5% respectively upon increase in the distance of submerged vanes from the inner bank. Furthermore, the values of $-\rho\overline{u'w'}$ and $-\rho\overline{u'v'}$ turbulence shear stresses at the outer bank in the case of installing the vanes at a distance of 40% of the channel width from the inner bank were smaller than those in the case of installing the submerged vanes at a distance of 60% of the channel width from the inner bank.

Keywords: Submerged Vanes; Position of Submerged Vanes at Width; Turbulence Shear Stress; Turbulence Kinetic Energy; The Secondary Flow Strength; 180 Degree Sharp Bend.

NOMENCLATURE

B	channel width
D	pier diameter
d_{50}	average particles diameter
d	sediment particles diameter
L_B	distance of submerged vanes from the inner bank
L_S	height of vanes on bed at the beginning of scour experiment
L_v	length of submerged vanes
R	central curvature radius
S_x	secondary flow strength
t_v	thickness of submerged vanes
Teta	degrees of curvature from the entrance to the end of the bend
u, v, w	instantaneous velocities respectively in longitudinal, transverse, and vertical directions
$\bar{u},\bar{v},\bar{w}$	average velocities respectively in longitudinal, transverse, and vertical directions
u',v',w'	fluctuating velocities respectively in longitudinal, transverse, and vertical directions
$u'_{rms},v'_{rms},w'_{rms}$	flow turbulence intensities respectively in longitudinal, transverse, and vertical directions
x, y, z	cartesian coordinates respectively in longitudinal, transverse, and vertical directions
y	upstream flow depth
α	horizontal angle of submerged vanes

1. INTRODUCTION

Turbulence is one the most important features of flow pattern in bends. It affects several river processes including erosion, sediment transport, bed morphology and the natural channel shape. Range of disorders in turbulent flows is so wide that no matter how much effort is made in order to replicate boundary conditions of the intended flow, the details of the flow will never be repeated. Although flow details cannot be precisely predicted per time and place, the turbulence phenomenon may be identified through its effects and properties, and be described in the framework of the same properties. Shear stress and kinetic energy are among parameters which may be mentioned as instances of turbulence phenomena. Reynolds stress may be employed in order to calculate shear stress by using the flow field and considering the conditions governing the phenomenon. Study of stress by using the Reynolds stress method is employed when velocity collection is conducted at a turbulent boundary layer. Therefore, the present study used the Reynolds stress method to measure bed shear stress at the bend. Prandtl (1952) classified the secondary flow into two groups: type 1 and type 2 secondary flows. Type 1 is a result of pressure, and type 2 a result of turbulence. Ippen and Drinker (1962) examined the flow present at the bend by injecting color matter and observed that thin color strings on channel bed moved towards the inner bend; whereas, those on water surface moved towards the outer bank. He defined such a phenomenon as the direct effect of wall friction on the whole flow field. Nouh and Townsend (1979) studied the influence of the secondary flow on bed shear stress distribution, and the length of such influence based on variations in shear stress. They concluded that not only did the effects of the generated secondary flow faded after passing the bend, but they also extended over a distance on the straight downstream path. Odgaard and Kennedy (1983) used submerged vanes with the aim of protecting banks at river bends through reduction of secondary flows eroding the outer banks of river bends. Blanckaert and Graf (1999) conducted a study of flow pattern and bed topography in curved channels with mobile bed in a bended flume with a central angle of 120 degrees. The results of their work indicated that velocity transverse vectors at the bend apex section vividly refer to presence of two cycles in opposite directions to each other. The larger cycle is called the central circular cell, a result of the centrifugal force created under the influence of channel curvature, and the other falls at the vicinity of the outer wall, and flows in the opposite direction of the main cycle. According to these two researchers and their study of normal and Reynolds shear stresses at that section of the channel, creation of such opposite-directed cycle is due to heterogeneity of the Reynolds vertical stresses inside the section. Lien *et al.* (1999) investigated the flow pattern in 90 and 180 degree bends by using the two-dimensional model averaged in depth. The effect of the secondary flow in this model has been considered through calculation of stress diffusion tensor. In addition to diffusion stresses, the important forces present along the channels have been compared, the result of which refers to presence of a stronger secondary flow in the 180 degree bend than in the 90 degree bend. Marelius and Sinha (2000) examined the optimum angle for the collision of the flow with the vane, and studied the flow pattern around a vane in a straight path with mobile bed both numerically and experimentally. Johnson *et al.* (2001) conducted 37 experiments and analyzed the effect of submerged vanes on prevention of scour at the marginal piers of the bridges through an experimental model. They observed that these vanes cause an increase in flow rate at the center of the channel, and a decrease in flow rate and shear stress on the margins. Czernuszenko and Rylov (2002) carried out a numerical investigation of the secondary flow mechanism in a straight open channel. They employed a simple model in order to demonstrate the presence of secondary flows generated by shear stress, and adopted Boussinesq's idea about viscosity of vortices in determination of turbulence stresses. Blanckaert and Graf (2002) investigated flow parameters on an erodible bed on a bended flume with a central angle of 120 degrees, and an average curvature radius of 2 meters. They used ADVP to study velocities in three directions, and their results indicated that turbulence shear stress values of $\rho\overline{u'w'}$ and $\rho\overline{u'v'}$ were lower at the outer bank than the respective values in a straight channel. Barbhuiya and Dey (2003) conducted an experimental study to examine instantaneous velocity components, turbulence intensity components, turbulence kinetic energy, and the Reynolds stresses around the cylindrical, vertical wall in a rectangular, straight channel by using ADV Acoustic-Doppler Velocimeter. Their results demonstrated generation of primary circular currents at the upstream side of the wall [11]. Blanckaert and Graf (2004) studied redistribution of velocity, boundary shear stress, and geometry and properties of bed topography in bended channels. They considered a central zone as a cell capable of rotation and a semi-three-dimensional model to determine bed morphology dynamics in bended channels. Wang and Cheng (2005) conducted a study of alterations in distribution of longitudinal velocity in channel and the Reynolds stress. The results indicated that flow quantities could be linearized, so that all such quantities may fall into two average components of flow base and fluctuations created via bed roughness. Accordingly, they proposed relations for velocity and the Reynolds stress under the influence of the secondary flows. Blanckaert and De Vrient (2005) used ADVP Acoustic-Doppler Velocity Profiler to investigate turbulent flow properties in a bended channel with a central angle of 120 degrees, and calculate kinetic energy and shear stress parameters. Soon-Keat *et al.* (2005) examined the flow pattern around a long vane in wide rivers with mobile beds. Rodriguez and Garcia (2008) employed an Accoustic-Doppler Velocimeter to study the secondary flow, flow turbulence properties, and transverse variations of the flow in a straight

channel. The results of this study reported the longitudinal velocity distribution including a number of organized centers of high flow velocity. Abad and Rhoalds (2008) examined the average and turbulence flow patterns in a meandering channel with rigid bed, and calculated such parameters as the Reynolds stress and turbulence kinetic energy at cross sections of that channel. The results of their study indicated that the center of the maximum flow velocity leaned towards the inner wall of the channel upon reaching the bend apex. Naji Abhari *et al.* (2010) conducted a study of variations in velocity components, stream lines, bed shear stress, and the secondary flow in a channel with a 90 degree bend. Their investigation demonstrated that local asymmetry in velocity components occurred due to presence of the secondary flow in a bended channel. Das *et al.* (2013a) employed an ADV velocimeter in an experimental study in a straight channel, and examined the flow pattern in the scour hole around a single cylindrical pier with three different diameters. Akib *et al.* (2014) investigated scour and flow pattern around group piers. Vaghefi *et al.* (2015) conducted an experiment in a 1-meter-wide channel with a 180 degree sharp bend and a central curvature of 2 in order to investigate velocity fluctuations, and then examine distribution of turbulence kinetic energy. The results of their study suggested that the maximum and the minimum turbulence kinetic energies occurred at the 85 and the 20 degree sections respectively. Further, the maximum longitudinal and transverse velocity fluctuations occurred at the 70 degree section near the inner wall. Vaghefi *et al.* (2016) used an ADV velocimeter in an experimental study, examined flow pattern, and calculated shear stress in a 180 degree sharp bend. The results suggested that the maximum shear stress occurred near the bed at the 40 degree angle. Haji Azizi *et al.* (2016) carried out a numerical investigation of the flow around a bridge pier in the presence of submerged vanes by using Fluent software. The results of their study indicated a desirable relationship between experimental and numerical results. Maatooq and Adhab (2017) analyzed the effect of the distance of the submerged vanes from the outer bank of the channel on sediment reach along the channel. To this aim, they installed the submerged vanes at different distances from the outer bank in a 180 degree bended channel. Dey *et al.* (2017) carried out an experimental investigation on the effect of different angles (10, 15, 20, 30, and 40 degrees) of submerged vanes in a 180 degree bend. The results of their efforts suggested that installation of the vanes at the 15 degree angle proved the most efficient in reducing scour at the outer bank. Vaghefi *et al.* (2018) studied scour around triad cylindrical series piers with a diameter of 5 cm in two cases, piers perpendicular to the flow and piers with a streamwise direction, under clear water conditions in a laboratory flume as wide as 100 cm with a 180 degree sharp bend. As reported in their study, with installations of the piers perpendicular to the flow and piers with streamwise direction, the largest area of scour hole around the piers occurred at the 60 degree angle, and sediment piles were observed at the downstream side of the piers. Abdi Chooplou *et al.* (2018) studied streamlines with average velocity alterations and the maximum velocity path around submerged vanes located at the upstream side of the bridge pier. Little effort has so far been made to understand variations of such stresses along the bend, which is due to two reasons. First, in the past three decades, there have been no precise instruments of measuring these parameters simultaneously, or they have been highly costly tools. Second, properties of flow turbulence are themselves highly unknown, and there are several uncertainties regarding analysis of the results. Therefore, this paper has tried to address the effect of installation of submerged vanes at the upstream side of the bridge pier on flow turbulence intensities, power of secondary flow, turbulence kinetic energy and shear stress in a 180 degree sharp bend.

2. MATERIALS AND METHODS

All experiments were conducted in a flume with a central angle of 180 degrees (U-shaped). A view of the laboratory flume, along with plan and cross section, is presented in Fig. 1(a).

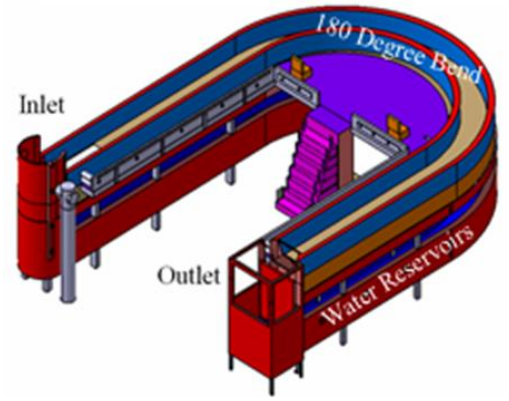

a

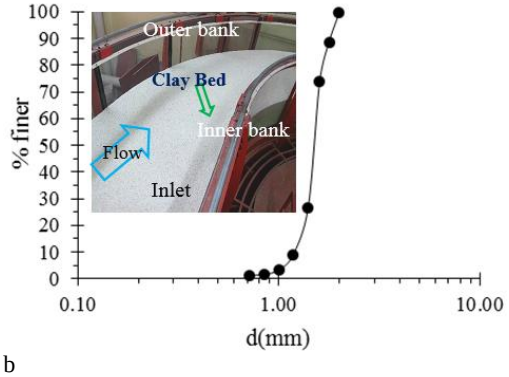

b

Fig. 1. (a) 3D view of the channel with dimensions, (b) gradation curve of the employed materials.

This channel consists of a 6.5-meter-long straight end upstream and a 5-meter-long straight end downstream, which have been connected to each

other with a 180 degree bend with an internal curvature radius of 1.5 m, and an external curvature radius of 2.5 m. The ratio of curvature radius to width (R/B) of the channel is 2. The 100-meter-wide channel (B) is 70 cm high. The bed of the channel is covered with graded sediments with an average diameter of 1.5 mm and a standard deviation of 1.14 mm up to the level of 30 cm.

The semi-log graph of materials gradation is illustrated in Fig. 1(b), where d denotes the diameter of bed materials in millimeters. According to suggestions given by previous researchers, the materials diameter should not be smaller than 0.7 mm so that ripple formation is prevented. $\frac{D}{d_{50}} \succ 20-25$ has also been recommended. D and d_{50} respectively represent the pier diameter and the average diameter of bed materials (Raudkivi and Ettema, 1983). The flow inlet discharge coefficient is 70 liters per second, and it is held constant during the experiment. The water level is also constant, equal to 18 cm, in the upstream straight path before entrance to the bend, and is set by the butterfly valve at the end of the downstream straight path. Scour experiments have been conducted under clear water and incipient motion conditions. During the experiments, the Froude number was 0.29 and the Reynolds number was approximately 51480. In scour experiments, a laser device was employed in order to measure the bed. After 9 hours, when the bed reached a relative balance, the balanced topography of the bed was measured. Using concrete adhesive, determination of the flow pattern on stabilized bed was made possible.

Measurement of velocity components and determination of the 3D pattern of the flow were done by using Vectrino velocimeter (ADV) . For a more precise measurement and a higher quality of flow pattern investigation, a greater number of sections were selected for measuring velocity. The side-looking probe helped measure the flow rate at areas in the vicinity of the channel walls and water surface, and the down-looking probe was used in other cases. Hence, the device collected 1500 flow velocity data per second in three directions.

Then, these data were converted into a format readable in Excel by using Explorer V software program. Figure 2 depicts the positioning of the velocimeter in the 180 degree bend. Two experiments were conducted by placing submerged vanes at a distance of 5 times the pier diameter in two positions: at distances of 40% (PFV) and 60% (PSV) of the channel width from the inner bank. The aforementioned submerged vanes were rectangular, made of 1-cm-thick Plexiglas sheets as long as 7.5 cm. At 75% submergence (4.5 cm above base level), they were placed at the 25 degree horizontal angle as is observed in Fig. 3. The bridge pier diameter was 5 cm, and it was installed at the 90 degree position.

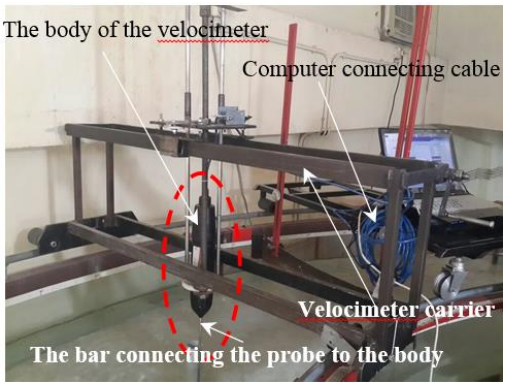

Fig. 2. Positioning of Vectrino velocimeter in the 180 degree sharp bend.

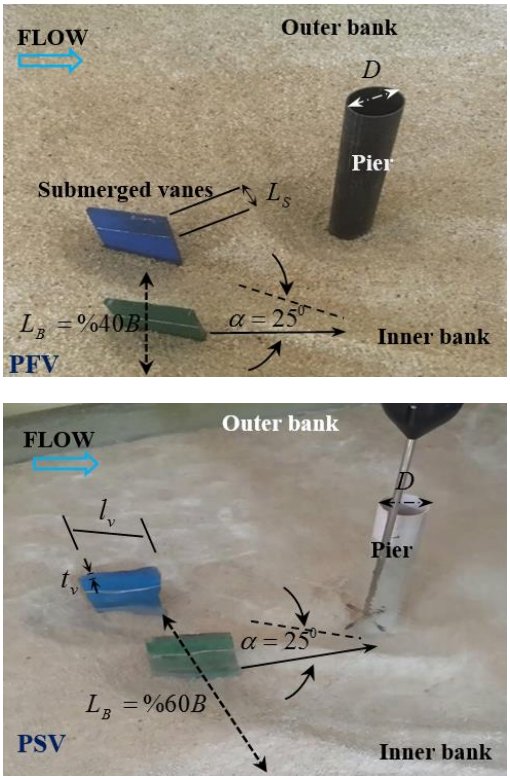

Fig. 3. Positioning of submerged vanes at the upstream side of the pier in the experiments.

3. RESULTS AND DISCUSSION

Turbulence intensity components, turbulence kinetic energy, shear stress distribution on bed, the secondary flow power, and topography alterations were examined in every experiment according to the flow pattern in open tracts and based on factors such as velocity vectors' distribution and 3D profiles. When the structure of turbulence along the bend is to be studied, analyzing "flow turbulence intensity" is indispensable. Flow turbulence intensities have been calculated as Root Mean Square (RMS) in different directions near the bed.

Considering the fact that the average velocity, fluctuating velocity, and flow turbulence parameters are obtained using instantaneous velocities, then the

relationship between such quantities is addressed as follows: According to Fig. 4, if quantitative temporal variations, such as velocity components, are recorded at a particular point in a turbulent flow field, average time values $(\bar{u},\bar{v},\bar{w})$ and instantaneous values (u,v,w) may be defined for the intended series. Therefore, fluctuating velocities (u',v',w') were obtained through the following relations. In a turbulent flow, due to random and irregular fluctuations of velocity, it is recommended that every velocity quantity be shown as the sum of an average time and a fluctuating member.

$$u = \bar{u} + u' \tag{1}$$

$$v = \bar{v} + v' \tag{2}$$

$$w = \bar{w} + w' \tag{3}$$

$$\bar{u} = \frac{1}{T}\int_0^T \mathrm{u}\,\mathrm{dt} \tag{4}$$

$$\bar{v} = \frac{1}{T}\int_0^T \mathrm{v}\,\mathrm{dt} \tag{5}$$

$$\bar{w} = \frac{1}{T}\int_0^T \mathrm{w}\,\mathrm{dt} \tag{6}$$

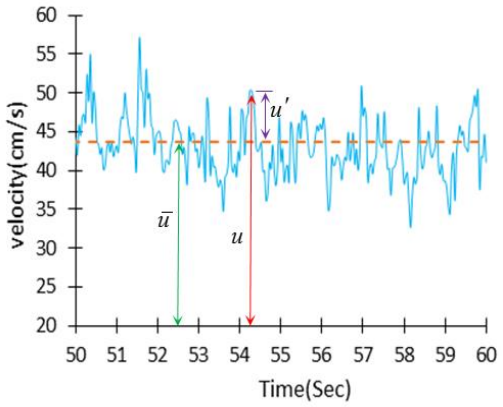

Fig. 4 An instance of time series of a longitudinal velocity component in a turbulent flow with definitions of its instantaneous and average time values.

By using the velocities measured by Vectrino velocimeter, the flow turbulence intensity may be calculated. The flow turbulence intensity is denoted in three directions: longitudinal, transverse, and vertical, respectively by $\sqrt{u'^2}$, $\sqrt{v'^2}$ and $\sqrt{w'^2}$. These turbulence intensities are obtained as RMS as follows (Das *et al.*, 2013b):

$$u'_{rms} = \left[\frac{1}{n}\sum_{i=1}^{n}(u_i - \bar{u}_i)^2\right]^{0.5} \tag{7}$$

$$v'_{rms} = \left[\frac{1}{n}\sum_{i=1}^{n}(v_i - \bar{v}_i)^2\right]^{0.5} \tag{8}$$

$$w'_{rms} = \left[\frac{1}{n}\sum_{i=1}^{n}(w_i - \bar{w}_i)^2\right]^{0.5} \tag{9}$$

Since investigation of flow turbulence at layers near the bed in open channels is highly important, given the creation of maximum bed shear stresses and the issue of bed scour, Fig. 5 presents turbulence intensity values of u'_{rms}, v'_{rms} and w'_{rms} in longitudinal, transverse, and vertical directions at a distance of 5% of the flow depth from the bed along the 180 degree sharp bend.

The red spectrum indicates a zone of high tension. According to Fig. 5, the maximum flow turbulence intensity occurs in longitudinal direction, largely at the area in the vicinity of the inner wall, ranging from the 60 to the 70 degree angles from the entrance of the bend. Whereas, other than this zone, which falls at a distance of 60% of the channel width from the inner bank, two other zones of higher turbulence intensities occur: one at the location of submerged vanes and the bridge pier, and the other at the downstream side of the piers at the end of the bend. It may be observed that a 20% displacement of submerged vanes in channel width towards the outer bank results in an increase in flow rate and shear stress at the outer bank (Fig. 5(a)).

A comparison between Figs. 5(b) and 5(c) demonstrates that the maximum transverse turbulence intensity is solely concentrated at areas near the bend apex, with the exception that the value and the zone of transverse turbulence intensity are larger than those of vertical turbulence intensity. In fact, upon reaching the bend apex, the center of the maximum flow turbulence intensity in transverse direction is directed towards the inner wall in PFV experiment; whereas, it is directed towards the outer wall in PSV experiment. To make a better and more precise comparision of the maximum flow turbulence intensity values in different directions, the maximum values of turbulence intensity, $u'_{rms}, v'_{rms}, w'_{rms}$, are shown in Fig. 6 at different cross sections along the 180 degree sharp bend in both experiments. In PSV experiment, it may be observed that the maximum value of flow turbulence occurs in longitudinal direction, and the minimum in vertical direction of the flow. On the other hand, in PFV experiment, the maximum value of flow turbulence occurs in transverse direction of the flow, which is 8% higher than that in PSV experiment. The other point worth of mention regarding Figs. 5 and 6 is the location of the maximum turbulence intensity.

According to these figures, the maximum flow turbulence intensity has occurred in transverse direction at the entrance of the bend, respectively at 84.5 and 86 degree cross sections; whereas, the maximum turbulence intensity in the other two

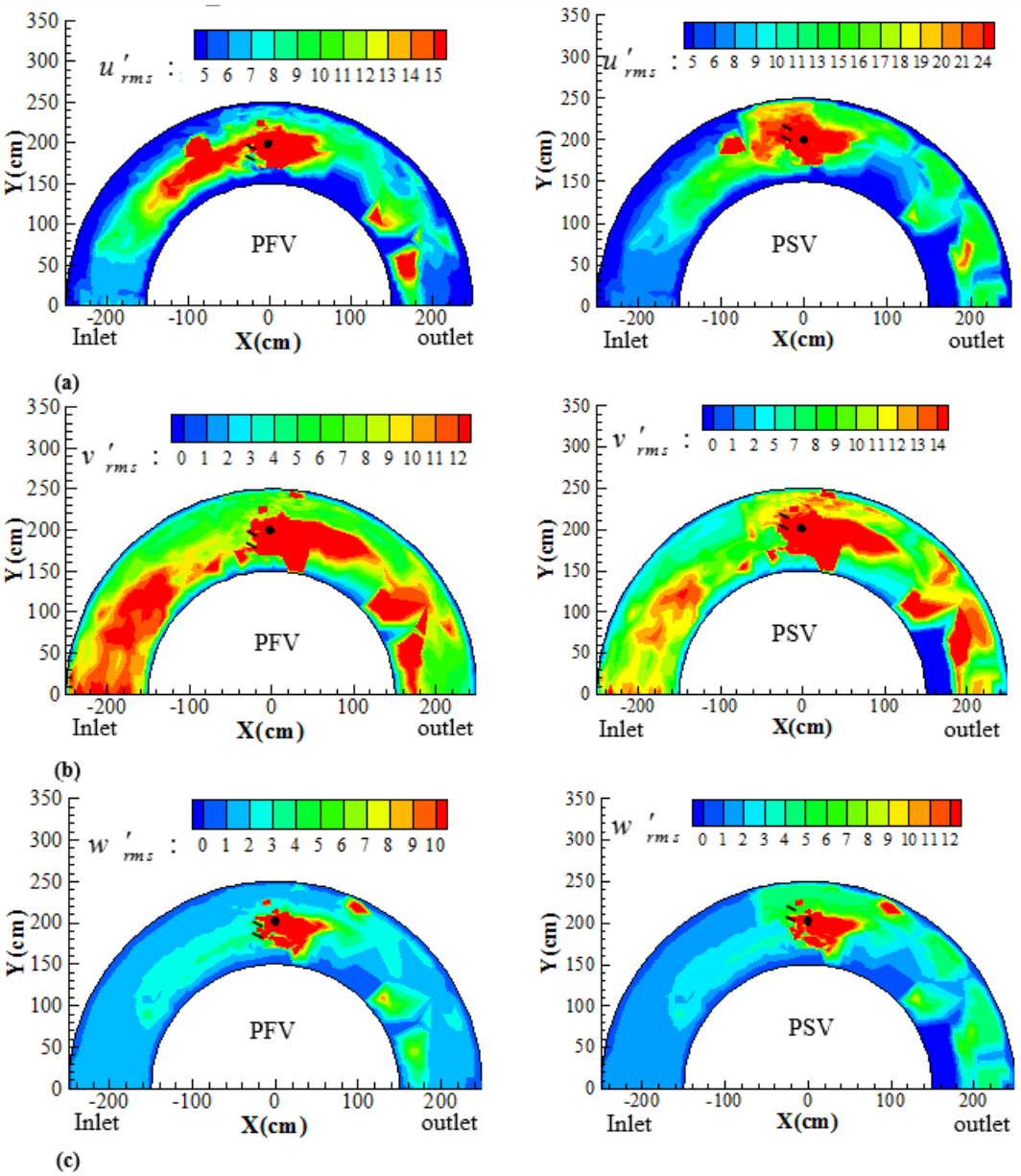

Fig. 5. Distribution of flow turbulence intensities (cm/s) **in the 180 degree sharp bend at a level equal to 5% of the flow depth from the bed in (a) longitudinal** u'_{rms} **, (b) transverse** v'_{rms} **, and (c) vertical** w'_{rms} **directions.**

directions (longitudinal and vertical directions) has moved to areas in the vicinity of the bend apex. As may be observed, the maximum values of longitudinal and vertical components of turbulence intensity increase by respectively 16 and 5.5% by increasing the distance between the submerged vanes and the inner bank. Transverse and vertical flow velocities demonstrating the secondary flows increase at the bend apex, the phenomenon which transports the maximum flow turbulence intensity from the 84 degree angle (near the bend entrance, where pressure gradients govern the secondary flows) to the area surrounding the structures located at the bend apex (where the influence of the secondary flow strength is significant).

Presence of the secondary flow results in alterations of velocity at different points along the bended path. Such velocity alterations near the bed are accompanied by shear stress variations. Therefore, Fig. 7 illustrates variations in the secondary flow power along the bend.

Based on Eq. (10) through (13), this value is defined as the ratio of the kinetic energy at the lateral section to the total kinetic energy of the main stream (Shukry, 1950).

$$Sx = \frac{k_{lateral}}{k_{main}} \tag{10}$$

$$Sx = \frac{\frac{V_{xy}^{2}}{2g}}{\frac{V^{2}}{2g}} \times 100 \quad (11)$$

$$Sx = \frac{V_{xy}^{2}}{V^{2}} \times 100 \quad (12)$$

$$Sx = \frac{v^{2}+w^{2}}{u^{2}+v^{2}+w^{2}} \times 100 \quad (13)$$

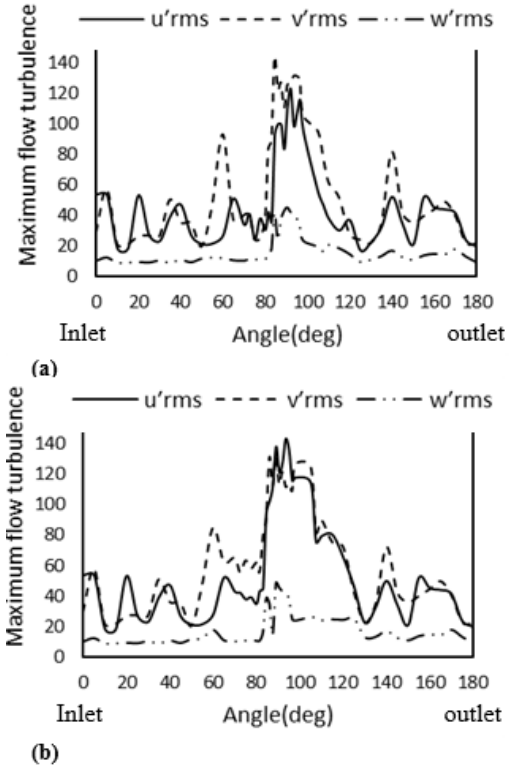

Fig. (6). Distribution of the maximum flow turbulence intensities (cm/s) **in longitudinal, transverse, and vertical directions in (a) PFV, and (b) PSV experiments.**

In the relation above, Sx denotes the secondary flow strength, V_{xy} is the resultant velocity in longitudinal and transverse directions, and V represents the resultant velocity in three directions. u, v, and w are velocity components in x, y, and z directions, and g denotes acceleration of gravity. One of the important factors intensifying erosion at bends, apart from shear stress, is the secondary flow strength (the vortex power). In general, when the flow enters the bend, the secondary flow strength along the bend has two maximum values, one at the bend apex and the other at the end of the bend. Considering the fact that the secondary flow strength is in correspondence with the square ratio of the components of the lateral flow to the main stream, waves increase from the entrance to the the vicinity of the submerged vanes, the phenomenon which eventually results in increase in hydraulic gradient, thus increasing the transverse velocity and the secondary flow strength. With the collision of the flow with vanes, a zone of return flows with low velocity is created, and causes a reduction in the secondary flow power. Thereafter, it has reached its maximum value at the bend apex, where the pier is located. At the onset of the experiment, the only factor influencing velocity alterations was section constriction due to presence of the bridge pier, and it is evident that velocity increases with a reduction in cross section. At the equilibrium time, with bed topography alterations fixed, section constriction due to presence of the pier, and increase in the area of scour hole are two opposite factors influencing velocity alterations. An investigation of velocity alterations reveals that this area has experienced reduction in tangential velocity and increase in the secondary flow power. Therefore, it may be concluded that the factor causing the increase in the scour hole area has overcome the factor causing section constriction, and has increased the secondary flow power. Thus, according to Fig. 7, it is possible to state that the secondary flow power has also increased around the pier where the maximum depth of scour hole occurs.

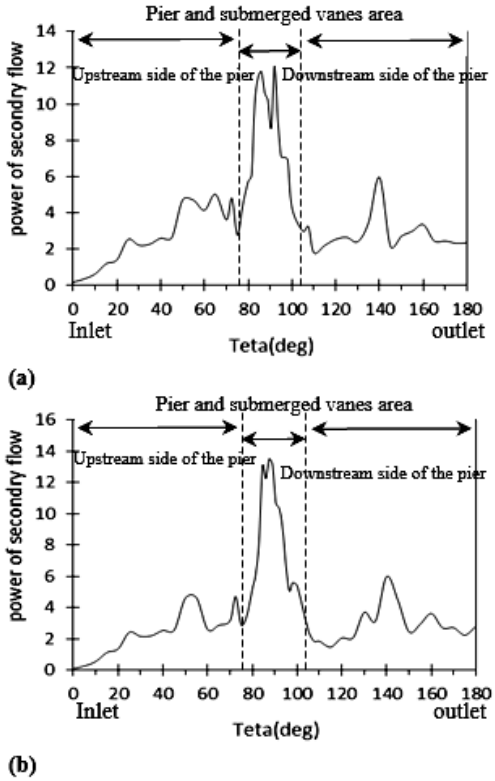

Fig. 7. Diagrams on the secondary flow strength throughout the bend in (a) PFV and (b) PSV experiments.

.In the case of placing the submerged vanes at distances of 40 and 60% of the channel width from the inner bank, the maximum secondary flow strength was 12.10 and 13.5%, and occurred at the

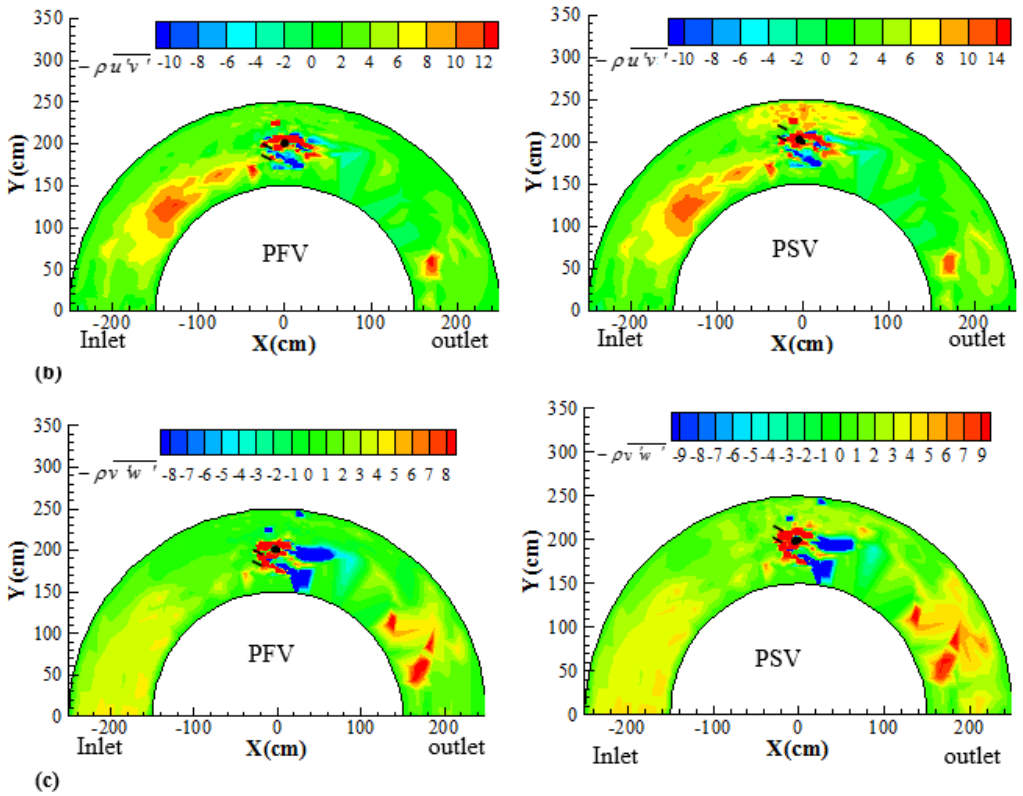

Fig. 8. Bed shear stress distribution $(gr/cm\times s^2)$ **in the 180 degree sharp bend at a level equal to 5% of the depth from the bed in (a) longitudinal, (b) transverse, and (c) vertical directions.**

92 and 87.5 degree cross sections from the entrance of the bend, respectively. In fact, a 20% displacement of the submerged vanes along the channel width towards the outer bank has increased the secondary flow strength around the pier by 11%, and moved it towards a location higher than the pier. From the bend apex to the 115 degree position, waves subside, and the secondary flow strength eventually decreases. Yet, from the 115 to the 145 degree position, the secondary flow strength increases due to beginning of the flow separation zone from the inner wall. As a result, the momentum is transported from the inner wall to the outer wall of the bend. The secondary flow strength decreases from the 145 degree position to the end of vector data field (straight path), because the lateral pressure gradient and the centrifugal force depreciate.

Figure 8 presents bed shear velocity distribution calculated via the Reynolds stress method at a level equal to 5% of the depth from the bed. The Reynolds shear stress may be calculated as follows (Das et al., 2013b) :

$$\tau_{zx} = -\rho\overline{u'w'} \tag{14}$$

$$\tau_{yx} = -\rho\overline{u'v'} \tag{15}$$

$$\tau_{zy} = -\rho\overline{v'w'} \tag{16}$$

where τ_{zx} denotes shear stress in z coordinate in x direction, τ_{yx} shear stress in y coordinate in x direction, and τ_{zy} shear stress in z coordinate in y direction. These stresses are obtained based on fluctuating velocity values. For instance,

$$\overline{u'v'} = \frac{1}{n}\sum_{i=1}^{n}(u-\bar{u})(v-\bar{v}) \tag{17}$$

As is seen in Fig. 8, the red spectrum illustrates the highly tensioned and positive zone in the bend. The powerfully tensioned zone has been specified in the bend under investigation, the zone which falls at the area of the structures located at the bend and in the middle of the bend. The turbulence shear stress values of $-\rho\overline{u'w'}$ at the bend apex are smaller in PFV experiment than the corresponding values in PSV experiment (Fig. 8(a)). It may be observed in Fig. 8(b) that the turbulence shear stress of $-\rho\overline{u'v'}$ at the bend entrance occurs from the vicinity of the inner wall to approximately the 75 degree angle. However, at the area from the 75 to the 100 degree angle, the maximum shear stress is transported to mid-channel, and in the vicinity of the submerged vanes in PSV experiment, it is transported to the outer half. The range of $-\rho\overline{u'v'}$ in the vicinity of the bridge pier has also increased, and the area under the influence of stress variations has expanded. According to Fig. 8(c), it may be observed that displacement of the submerged vanes along the channel width has not altered the location

of $-\rho\overline{v'w'}$, and increase in the distance between the submerged vanes and the inner bank has increased its maximum value by 10%. A comparison between Figs. 8(a) through (8c) refers to the fact that in all installations of the submerged vanes at the upstream side of the pier, towards the inner bank of the submerged vanes and the pier, the value of $-\rho\overline{u'v'}$ is negative; whereas, the value of $-\rho\overline{v'w'}$ near the outer wall and the downstream side of the channel has become negative. Turbulence shear stress values of $-\rho\overline{u'w'}$ and $-\rho\overline{u'v'}$ at the outer bank in PFV experiment are smaller than the corresponding values in PSV experiment. Furthermore, the turbulence shear stress of $-\rho\overline{v'w'}$ refers to cross sectional cells' rotation and is maximum at the eye of the cell.

The following relation is employed in order to calculate the turbulence energy. In fact, "TKE" represents the amount of kinetic energy resulting from velocity fluctuations or turbulence (Das *et al.*, 2013b) .

$$TKE = 0.5(\overline{u'^2} + \overline{v'^2} + \overline{w'^2}) \tag{18}$$

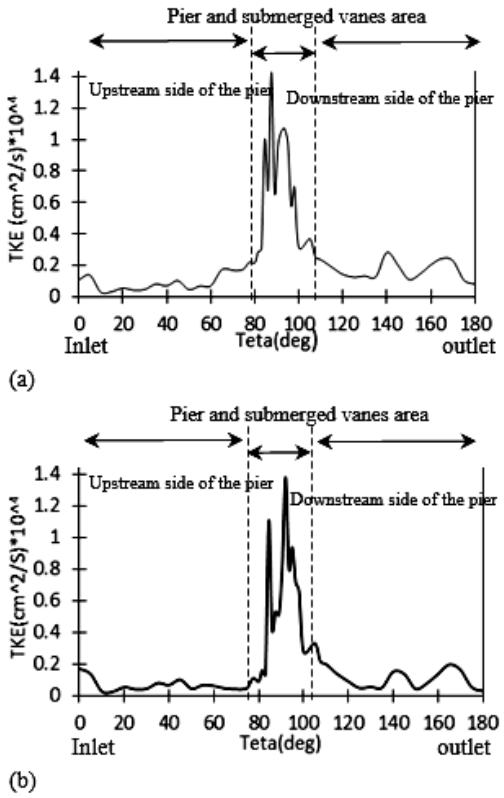

Fig 9. Maximum values of turbulence kinetic energy (cm^2/s) **throughout the bend in (a) PFV, and (b) PSV experiments.**

Figure 9 presents the maximum values at different angles along the bend in order to investigate the calculated values of turbulence kinetic energy along the bend. According to this figure, it may be concluded that the maximum value of the turbulence kinetic energy along the bend occurs in the 92 degree position in PFV experiment, while it occurs in the 87.5 degree position from the entrance of the bend in PSV experiment, distances which are respectively 1.37×10^4 and 1.43×10^4 cm^2/s. Values of turbulence kinetic energy were lowest at initial sections of the bend; hence, it is observed that its minimum values occur in PFV and PSV experiments at respectively 15 and 10 degree positions.

Figure 10 depicts qualitative streamline patterns in the 25, 55, 90, 135, 155, and 175 degree angles in PFV and PSV experiments. According to Fig. 10(a), the streamlines in the 25 degree angle are evidently directed towards the inner wall of the channel. Figs. 10(b) and 10(c) clearly demonstrate a higher deviation towards the inner wall compared to other figures.

Based on Fig. (5), the zone of the maximum turbulence intensity may be attributed to intense deviation of streamlines towards the inner bend in Figs. 10(b) and 10(c).

This also holds true at the downstream area of the piers as well as the second half of the bend in Figs. 10(d) and 10(e) at a lower intensity. Eventually, inclination of the streamlines towards the inner bank has decreased at the bend outlet, and the flow path extends towards the outlet of the bend (Fig. 10(f)). It may generally be suggested that in all of these figures, the orange ribbon refers to the layer near the bed, which demonstrates inclination of the streamlines towards the inner wall of the channel throughout the bended path. This indicates the longitudinal pressure gradient governing the secondary flows at the layer near the bed in the 180 degree sharp bend, the fact which has led to increase in, and in fact, concentration of flow turbulence intensity in the vicinity of the inner wall of the bend.

The scour mechanism mostly occurs under the influence of the maximum velocity and a higher shear stress. Since velocity, and consequently the maximum shear stress, at the apex of the sharp bend occur around the submerged vanes and the bridge pier, scouring occurs at this area. Given the different positions of the submerged vanes along the channel width, bed topography alterations in the two experiments also differ.

Figure 11 illustrates bed topography in PFV and PSV experiments accompanied by 3D magnifications of the area around the pier and the submerged vanes as a result of the scour experiment. Occurrence of sedimentation at the inner bank, and scour around the structures can be observed.

The span of scour hole in PSV experiment has a higher inclination towards the outer bank than that in PFV experiment. Transportation of sedimentation from the inner wall to the channel axis and the outer wall around the outlet of the bend may be observed in this figure.

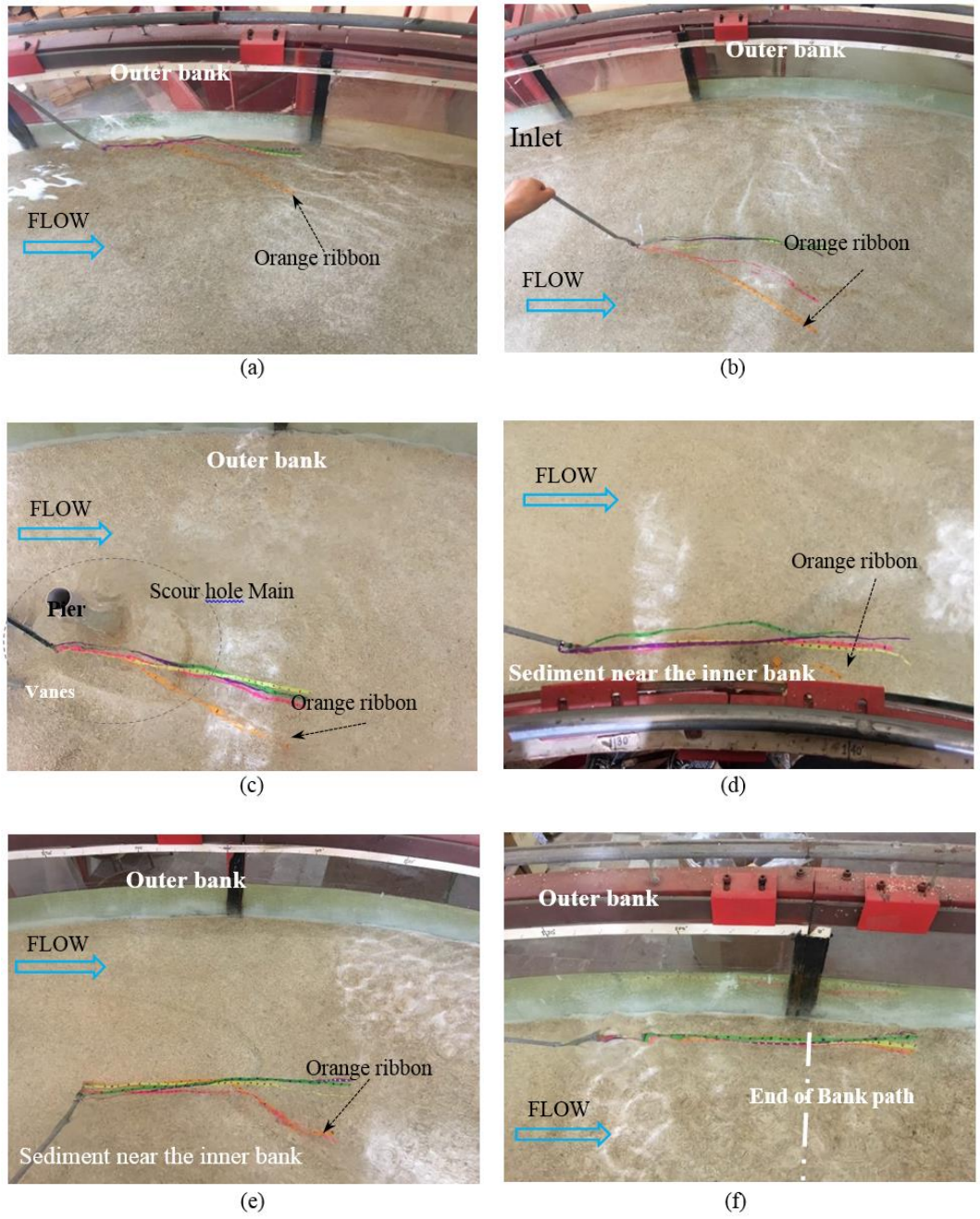

Fig. 10. A view of the qualitative flow pattern using orange ribbons at different cross sections in the 180 degree sharp bend at (a) 25, (b) 55, (c) 90, (d) 135, (e) 155 degrees, and (f) the end of the bend.

4. CONCLUSION

The following may be stated as the most important findings of this paper.

- The zone of the maximum transverse and vertical turbulence intensities has only been concentrated at the areas near the bend apex, except that the value and the zone of transverse turbulence intensity are higher than those of vertical turbulence intensity.
- Upon reaching the bend apex, the center of the maximum flow turbulence intensity in transverse direction inclines towards the inner wall in PFV experiment, and towards the outer wall of the channel in PSV experiment.
- The maximum value of turbulence kinetic energy along the bend occurs at the 92 degree section in PFV experiment, while it occurs at the 87.5 degree section from the beginning of the bend in PSV experiment.
- The minimum values of turbulence kinetic energy in PFV and PSV experiments occur at respectively 15 and 10 degree cross sections.

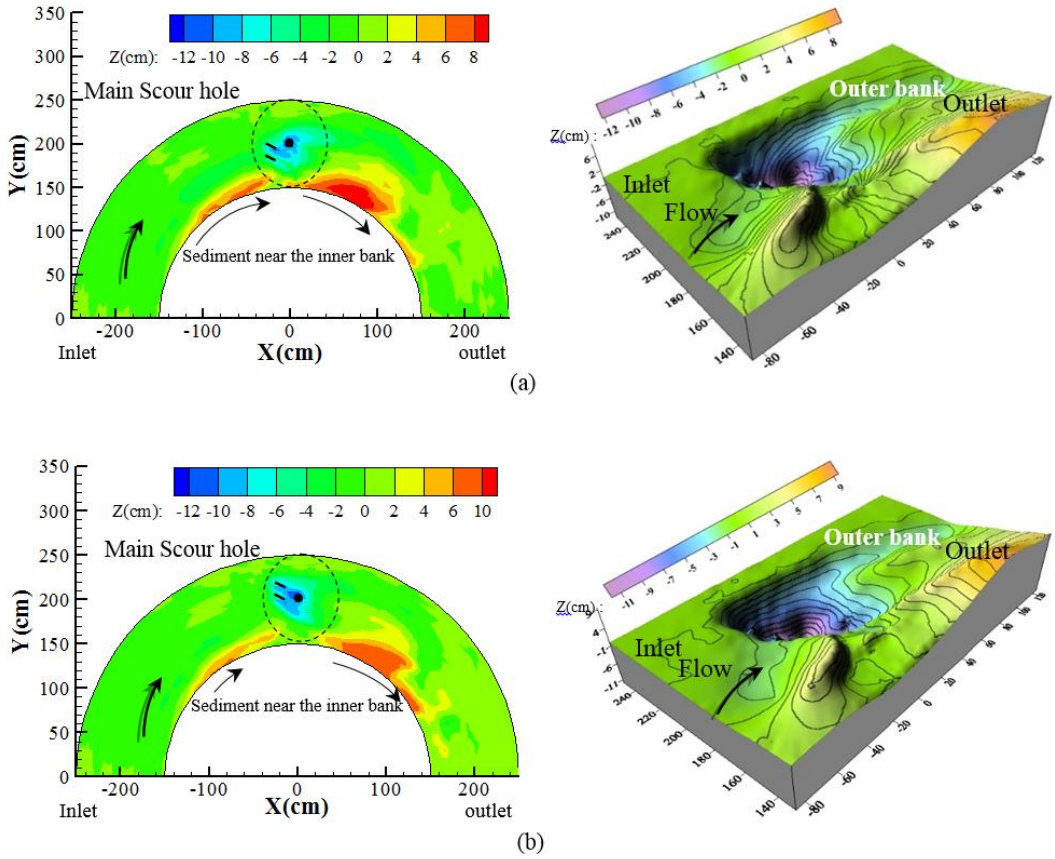

Fig. 11. Bed topography in (a) PFV, and (b) PSV experiments accompanied by 3D magnifications of the area around the pier and the submerged vanes.

- With a 20% displacement of the submerged vanes along the channel width towards the outer bank, the maximum value of the secondary flow strength around the pier has increased by 11%.
- The turbulence shear stress of $-\rho\overline{u'v'}$ at the bend inlet occurs near the inner wall. This lasts until the 75 degree angle, and then the center of the turbulence shear stress is transported to the outer half at the area of the submerged vanes in PSV experiment.
- The range of $-\rho\overline{u'v'}$ near the bridge pier has increased and the area under the influence of stress variations expands.
- Displacement of the submerged vanes along the channel width has not created any change in the location of $-\rho\overline{v'w'}$ turbulence shear stress, and by increasing the distance between the submerged vanes and the inner bank, its maximum value increases by 10%.
- The values of $-\rho\overline{u'w'}$ and $-\rho\overline{u'v'}$ turbulence shear stresses at the outer bank in PFV experiment are smaller than the corresponding values in PFV experiment.

REFERENCES

Abad, J. D. and B. L. Rhoalds (2008). Flow structure at different stages in a meander-bend with bend way weirs. *Journal of Hydraulic Engineering* 134(8), 1052-1063.

Abdi Chooplou, Ch., M. Vaghefi and S. H Meraji (2018). Study of Streamlines under the Influence of Displacement of Submerged Vanes in Channel Width, and at the Upstream Area of a Cylindrical Bridge Pier in a 180 Degree Sharp Bend. *Journal of Hydraulic Structures* 4(1), 55-74.

Akib, S., A. Jahangirzadeh and H. Basser (2014). Local scour around complex pier groups and combined piles at semi-integral bridge. *Journal of Hydrology and Hydromechanics* 62(2), 108-116.

Barbhuiya, A. K. and S. Dey (2003). Measurement of turbulent flow field at a vertical semicircular cylinder attached to the side wall of a rectangular channel. *Flow measurement and Instrumentation* 15(2), 87-96

Blanckaert, K. and H. J. De Vriend. (2005). Turbulence characteristics in sharp openchannel bends. *Physics of Fluids* 17(5), 055102-1-055102-15.

Blanckaert, K. and W. H. Graf (2002). Mean flow and turbulence in open-channel bend. *Journal of Hydraulic Engineering* 127(10), 835-847.

Blanckaert, K. and W. H. Graf (2004). Momentum transport in sharp open-channel bends. *Journal of Hydraulic Engineering* 130(3), 186-198.

Blanckaert, K., and W. H. Graf (1999). Outer- bank cell of secondary circulation and boundary shear stress in open- channel bends. Proc. *1st RCEM Symp. Genova, Italy, I*: 533-543.

Czernuszenko, W. and A. Rylov (2002). Modeling of three-dimensional velocity field in open channel flows. *Journal of Hydraulic Research* 40(2), 135-143.

Das, S., R. Das and A. Mazumdar (2013a). Circuation characteristics of horseshoe vortex in scour region around circular piers. *Water Science and Engineering* 6(1), 69-77.

Das, S., R. Das and A. Mazumdar (2013b). Comparison of characteristics of horseshoe vortex at circular and square piers. Research Journal of Applied Sciences, *Engineering and Technology*, 5(17), 4373-4387.

Dey, L., A. K. Barbhuiya and P. Biswas (2017). Experimental study on bank erosion and protection using submerged vane placed at an optimum angle in a 180 laboratory channel bend. *Geomorphology* 283, 32-40.

Haji Azizi, S., F. Davood, A. Hadi and A. Akram (2016). Numerical Simulation of Flow Pattern around the Bridge Pier with Submerged Vanes. *Journal of Hydraulic Structures* 2(2), 46-61.

Ippen, A. T. and P. A. Drinker (1962). Boundary shear stresses in curved trapezoidal channels. *Journal of the Hydraulics Division* 87(6), 143-179.

Johnson, P.A., R. D. Hey, M. Tessier and D.L. Rosgen (2001). Use of vanes for control of scour at vertical wall abutments. *Journal of Hydraulic Engineering. ASCE* 127(9), 772-778.

Lien, H.C., T. Y. Hsieh, J. C. Yong and K. C. Yeh (1999). Bend-Flow Simulation Using 2D Depth-Averaged Model. *Journal of Hydraulic Engineering* 125(10), 1097–1108.

Maatooq, J. S. and B. Adhab (2017). Effect of Distance of the Submerged Vanes from the Outer Bank on Sediment Movement within 180 Bend. *American Journal of Engineering and Applied Sience* 10(3), 679-683.

Marelius, F. and S. K. Sinha (1998). Experimental Investigation of Flow past Submerged Vanes. *Journal of Hydraulic Engineering* 124(5), 542 – 545.

Naji Abhari, M., M. Ghodsian, M. Vaghefi and N. Panahpur (2010). Experimental and numerical simulation of flow in a 90° degree bend. *Flow Measurment and Instrumentation* 21(3), 292-298.

Nouh, M. and R. D. Townsend (1979). Shear-stress distribution in stable channel bends. *Journal of the Hydraulics Division 105*(10), 1233-1245.

Odgaard, A.J. and J. F. Kennedy (1983). River-Bend Bank Protection by Submerged Vanes. *Journal of Hydraulic Engineering* 109(8), 1161-1173.

Prandtl, L. (1952). *The essentials of fluid dynamics*. Blackie & So, London, United Kingdom.

Raudkivi, A. J. and R. Ettema (1983). Clear-Water scour at Cylindrical Piers. *Journal of Hydraulic Engineering* 125(1), 59-66.

Rodriguez, J. F. and M. H. Garcia (2008). Laboratory measurements of 3-D flow patterns and turbulence in straight open channel with rough bed. *Journal of Hydraulic Research* 46(4), 454-465.

Shukry, A. (1950). Flow around Bends in an open Flume. *Transactions of the American Society of Civil Engineers* 115(1), 751-779.

Soon-Keat, T., Y. U. Guoliang, L. Siow-Yong and O. Muk-Chen (2005). Flow structure and sediment motion around submerged vanes in open channel. *Journal of waterway, port, coastal, and ocean engineering* 131(3), 132-136.

Vaghefi, M., M. Akbari and A. R. Fiouz (2015). Experimental Study of Turbulence Kinetic Energy and Velocity Fluctuation Distributions in a 180 Degree Sharp Bend, 10th *International Congress on Civil Engineering*, University of Tabriz, Tabriz.

Vaghefi, M., M. Akbari and A. R. Fiouz (2016). An experimental study of mean and turbulent flow in a 180 degree sharp open channel bend: Secondary flow and bed shear stress KSCE. *Journal of Civil Engineering* 20(4), 1582-1593.

Vaghefi, M., M. J. T. N. Motlagh, S. Sh. Hashemi and S. Moradi (2018). Experimental study of bed topography variations due to placement of a triad series of vertical piers at different positions in a 180° bend. *Arabian Journal of Geosciences* 11(5), 102.

Wang, Z. Q. and N. S. Cheng (2005). Secondary flows over artificial bed strips. *Advances in Water Resources* 28(5), 441-450.